Chinese Chemical Letters 33 (2022) 4756–4760

Contents lists available at ScienceDirect

Chinese Chemical Letters

journal homepage: www.elsevier.com/locate/cclet

The role of Cs dopants for improved activation of molecular oxygen and degradation of tetracycline over carbon nitride

Qian Liu[a], Hui Li[b], Hao Zhang[b], Zhurui Shen[b,*], Huiming Ji[a]

[a] School of Materials Science and Engineering, Key Laboratory of Advanced Ceramics and Machining Technology, Ministry of Education, Tianjin University, Tianjin 300350, China
[b] School of Materials Science and Engineering, Nankai University, Tianjin 300350, China

ARTICLE INFO

Article history:
Received 27 September 2021
Revised 29 October 2021
Accepted 31 December 2021
Available online 7 January 2022

Keywords:
O_2 activation
Reactive oxygen species
Cs doping of CN
Degradation and mineralization
Tetracycline

ABSTRACT

Molecular oxygen (O_2) is activated to reactive oxygen species (ROS) by transferring energy and carriers in the photocatalytic process, which plays an important role in environmental remediation. Herein, Cs-doped carbon nitride (CN-*x*Cs, x = 0.2, 0.8, 1) was prepared by CsCl directly inducing the structural reconstruction of carbon nitride (CN), which had obvious molecular oxygen activation ability to promote tetracycline (TC) degradation. Besides, we explored the influence of Cs doping concentration. As a consequence, the doping concentration of Cs was an important factor affecting the activation of O_2, which could cause changes in the physical and chemical structure of CN, make O enter the CN structure, form N vacancy defects and cyano groups. In addition, a proper amount of Cs doping could reduce the band gap value, increase the light absorption range, have better charge separation and transfer performance, which could remarkably promote the activation of O_2. Benefiting from these advantages, CN-0.8Cs could generate a higher concentration of superoxide radicals ($^{\bullet}O_2^-$, 179.30 μmol/L), which was much higher than CN (6.22 μmol/L). Therefore, it exhibited excellent TC degradation photocatalytic performance, and the rate constant k of TC degradation was 0.020 min^{-1}, which was 6.7 times the degradation rate of CN (k = 0.0030 min^{-1}). Furthermore, the possible degradation pathways of TC were proposed based on the results of HPLC-MS.

Molecular oxygen (O_2) is a common oxidant with relatively stable performance and rich content (21% in the air), which is considered the most environmentally friendly and economical oxidant [1,2]. However, it is difficult for O_2 to directly oxidize some common organic pollutants in the natural environment. In this case, it is an effective method to reduce O_2 to ROS with high activity through electrons generated by photocatalytic technology [3,4]. ROS is a one-electron reduction product of oxygen, which mainly includes superoxide anion radical ($^{\bullet}O_2^-$), hydroxyl radical ($^{\bullet}OH$), singlet oxygen ($^1O_2$), hydrogen peroxide (H_2O_2) and so on. In addition, the activation of molecular oxygen by the semiconductor photocatalyst not only has the advantages of low energy consumption and high efficiency, but also proved to be one of the greenest and most effective environmental remediation strategies [5,6]. Therefore, it is most critical to choose a suitable photocatalyst for activating molecular oxygen.

Carbon nitride (CN) is a non-metallic layered material, which has become a favorable candidate for photocatalyst due to its low cost, high stability, nontoxic and harmless, easy to synthesize and modify [7–10]. Because of its good conduction band position and molecular oxygen adsorption capacity, it has attracted widespread attention in the field of molecular oxygen activation [11–14]. Therefore, researchers have used various methods such as heterojunction construction, noble metal loading, element doping and other modification methods to further improve its molecular oxygen activation ability [15–18]. In recent years, many studies have reported improving the photocatalytic efficiency of CN by doping with alkali metal elements [19–22]. It is found that alkali metal halides can reduce the in-plane long-range periodicity order of CN, and larger cationic ions have a more significant effect [23]. It also has been reported that as the atomic number of the doped alkali metal increases, the band gap value of CN continues to decrease, the separation and transfer efficiency of electrons is further improved, and the photocatalytic activity is enhanced [24–26]. Although Cs is a stable alkali metal element with the largest atomic number, there are few reports on the effect of Cs doping on the photocatalytic performance of CN. Consequently, we

* Corresponding author.
E-mail address: shenzhurui@nankai.edu.cn (Z. Shen).

https://doi.org/10.1016/j.cclet.2021.12.089
1001-8417/

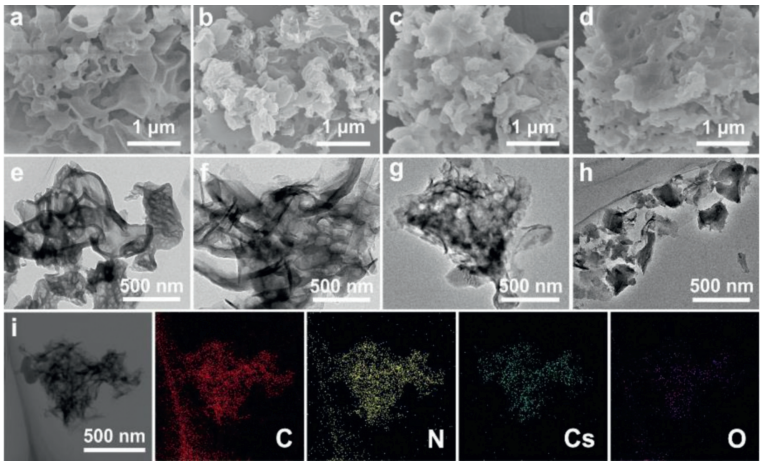

Fig. 1. SEM images (a-d) and TEM images (e-h) of CN, CN-0.2Cs, CN-0.8Cs and CN-1Cs, (i) is the element mapping of CN-0.8Cs (including C, N, Cs, O elements).

prepared Cs-doped carbon nitride (CN-*x*Cs, $x = 0.2, 0.8, 1$) with CsCl as a Cs source. The analysis indicated that the introduction of Cs could induce CN structure reconstruction, make O enter the CN structure, form N vacancy defects and cyano groups, which could promote the activation of molecular oxygen [11]. Furthermore, it could effectively reduce the band gap value, increase the light absorption range, and have better charge separation and transfer performance, so it could significantly promote the generation of $^{\bullet}O_2^-$. CN-0.8Cs had a strong O_2 activation ability, which greatly promotes the degradation ability of tetracycline. After 100 min, it showed the best tetracycline (TC) degradation efficiency. The contributions of $^{\bullet}O_2^-$, $^{\bullet}OH$ and h^+ in the degradation process were calculated, which were 90%, 45%, and 10%, respectively. This study intends to investigate the influence of the doping of alkali metal Cs on the structure and performance of CN, which is of great significance for the photocatalytic molecular oxygen activation for the realization of the oxidation reaction of pollutant organic molecules.

The formation process of CN-*x*Cs was shown in Fig. S1 (Supporting information). Briefly, Urea was heated to 500 °C to form a melon structure CN [27] characterized by N−H bridges and structural hydrogens in the form of terminal amino groups. Then, the degree of polymerization of CN became higher at 550 °C, the tris-triazine ring formed a regular network structure. Moreover, under the influence of CsCl, the chemical structure of CN was reconstructed by breaking the hydrogen bond and deamination, so that Cs and O entered the CN structure to form N vacancy defects and cyano groups.

The micromorphology of CN and CN-*x*Cs could be observed through SEM and TEM images (Fig. 1). CN was made up of a messy accumulation of many nanoflakes, and its surface had holes caused by gas generation during the urea polymerization process, and low-concentration Cs doping had basically no effect on the morphology of CN-0.2Cs. On the contrary, the thickness of nanosheets in CN-0.8Cs and CN-1Cs samples increase, while the size decreased. TEM images showed that the reason for the thickening of the nanosheets was the interaction between the CN layers, resulting in the formation of a layered agglomerate structure that was difficult to separate. Furthermore, EDS-mapping showed that CN-0.8Cs contained C, N, Cs and a small amount of O elements, indicating that Cs elements were successfully doped into CN and caused a part of O to enter the CN framework.

The specific surface area and pore size distribution of the sample were calculated using the nitrogen adsorption and desorption curve. As shown in Fig. S2a (Supporting information), all samples exhibited type IV isotherms. The BET specific surface area of each sample was shown in Table S2 (Supporting information). As the doping concentration increases, the specific surface area of the sample decreased slightly. It is supposed that the size of the nanosheets after Cs doping decreased and the hole structure disappears, and the lamellar stacking occurred, which corresponded to the results of SEM and TEM. As shown in Fig. S2b (Supporting information), the pore size distribution calculated by the BJH method showed that Cs doping did not have much effect on the pore size of the sample. The XRD patterns of CN and CN-*x*Cs were shown in Fig. S3 (Supporting information). The (100) peak of CN was at 13.2°, which was related to the in-plane repetition of the 3-*s*-triazine unit, and the (002) peak at 27.3° represented the stacking of the interlayer aromatic system [28]. With the increase of Cs doping concentration, the (100) peak weakened to disappear, which might be due to the decrease of the nanosheets and the destruction of the tri-*s*-triazine ring [29]. The (002) peak shifted towards high angles and became sharp, indicating that the doping of Cs might coordinate with N or O atoms to enhance the interaction between adjacent layers and reduce the layer spacing [30,31].

XPS was used to characterize the surface chemical state of the sample. As shown in Fig. 2a, the C 1s, N 1s, and O 1s signals showed three sharp peaks at 288.4, 399.6, and 533.8 eV in the spectrum. CN-*x*Cs showed Cs 3d signal peaks at 724.8 and 738.6 eV in Fig. 2b, indicating that Cs was successfully doped. As the doping concentration of Cs increased, the signal intensity and the atomic percentage of Cs increased (Table S3 in Supporting information). There was no Cl 2p peak in the spectrum, indicating that Cs was doped into CN-*x*Cs instead of CsCl (Fig. 2c). After Cs doping, the surface atomic ratio of C to N increased from 0.9 of CN to 2.3 (Table S3), indicating that N vacancies appeared, and the content of N vacancies increased with the increase of doping concentration. For further research on the types of N vacancies, the N 1s fine spectrum was tested. As shown in Fig. 2d, the N 1s spectrum had four peaks at 398.5, 399.5, 400.9 and 404.0 eV, corresponding to the two coordinate nitrogen atoms (N_{2C}), three coordinate nitrogen (N_{3C}), NH_x group and charge effect [32]. As shown in Table S4 (Supporting information), compared with CN, the atomic percentage of N_{3C} in CN-*x*Cs decreased from 27.2% to 14%, indicating a decrease in N_{3C} content. On the contrary, the N_{2C} content increased from 49.9% to 77.2%. This might be due to the formation of cyano groups (−C≡N), whose binding energy was between N_{2C} and N_{3C}, causing the cyano group peak to overlap with the N_{2C} peak [22]. It also can be seen from the C 1s spectrum given in Fig. 2e that the peaks at 284.8, 286.1 and 288.1 eV correspond to C−C, C−NH_x and N=C−N, respectively [33]. With the increase of doping concentration, the content of N=C−N kept decreasing, while C−NH_x

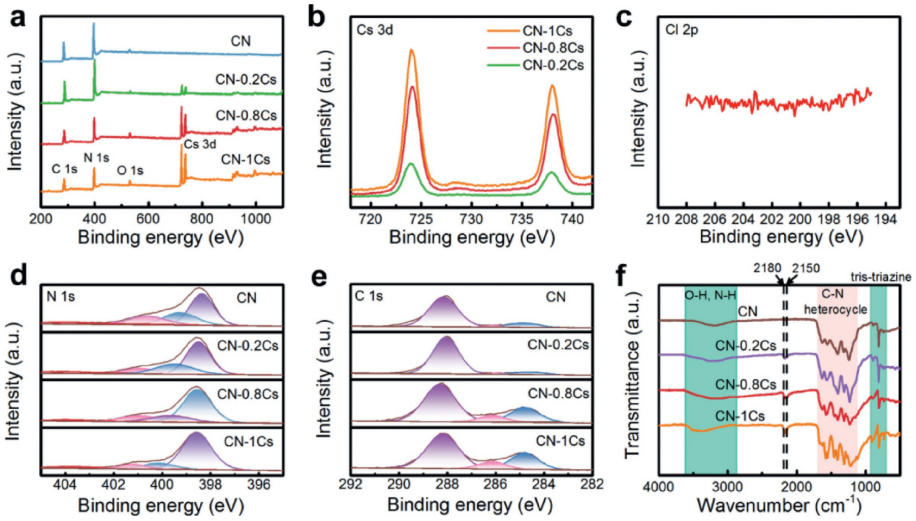

Fig. 2. (a) XPS survey spectrum of CN and CN-*x*Cs, the high-resolution XPS spectra expanded for the (b) Cs 3d, (c) Cl 2p, (d) N 1s and (e) C 1s of CN and CN-*x*Cs, and (f) FTIR spectra of CN and CN-*x*Cs.

kept increasing (Table S5 in Supporting information). These results suggested that during the reaction between CsCl and CN, the N_{3C} between the tri-*s*-triazine rings was attacked to form N_{3C} vacancies, and destroyed the tri-*s*-triazine ring in-plane arrangement. What's more, the Cs doping caused the tri-*s*-triazine heterocycle to be opened, resulting in generating a cyano structure, and increasing the number of O atoms, reducing the content of N=C–N and forming more C–NH_x groups. A part of Cs replaced the proton H of the NH_x group at the end of the triazine ring, which reduced the NH_x content from 22.9% to 8.8% (Table S4). FTIR spectroscopy was used to further detect the chemical exhibited similar characteristic bands, which were represented by three parts. As shown in Fig. 2f, the region of 800 cm^{-1} was considered to be the vibration mode of the triazine unit, while the 1200–1800 cm^{-1} region was attributed to the stretching vibration mode of aromatic CN heterocycles [26]. There was a wide absorption band at 3000–3600 cm^{-1}, which was caused by the overlap of the vibration peaks of the hydroxyl group –OH, adsorbed water and the surface amine group –NH [32]. Furthermore, Cs doped CN showed two new peaks at 2150 and 2180 cm^{-1}. These two peaks could be ascribed to the destruction of the tri-*s*-triazine ring structure by Cs. O entered the CN framework to form a C–O groups (2150 cm^{-1}) [34], and –C–NH_2 was deprotonated to form –C≡N (2180 cm^{-1}) [35]. In particular, the appearance of the –C≡N confirmed the opening of the triazine heterocycle and confirmed the assumption of the existence of the –C≡N in the XPS analysis results.

The doping of Cs changed the band structure and electronic properties of CN, thereby affecting the light absorption performance and charge separation process of CN. UV–vis DRS gave the absorption edge of the sample so as to study the energy band structure of the prepared sample in Fig. 3a. With the increase of Cs doping concentration, the absorption edge shifted red, indicating that Cs doping can broaden the light absorption range. The corresponding band gap value (E_g) of CN, CN-0.2Cs, CN-0.8Cs and CN-1Cs were 2.62, 2.58, 2.48 and 2.45 eV, respectively (Fig. 3b). In addition, the valence band potential (E_{VB}) was determined by the VB XPS spectrum (Fig. 3c). The E_{VB} of CN, CN-0.2Cs, CN-0.8Cs, and CN-1Cs were 1.95, 1.97, 2.09, and 2.11 V, respectively. Besides, the conduction band potential (E_{CB}) of the sample could be calculated by the formula $E_{VB} = E_g + E_{CB}$. The E_{CB} of CN, CN-0.2Cs, CN-0.8Cs and CN-1Cs were −0.67, −0.61, −0.39 and −0.34 V, respectively. According to the above results, their band structure was shown in Fig. 3d. The reason for the downward shift of the valence band and

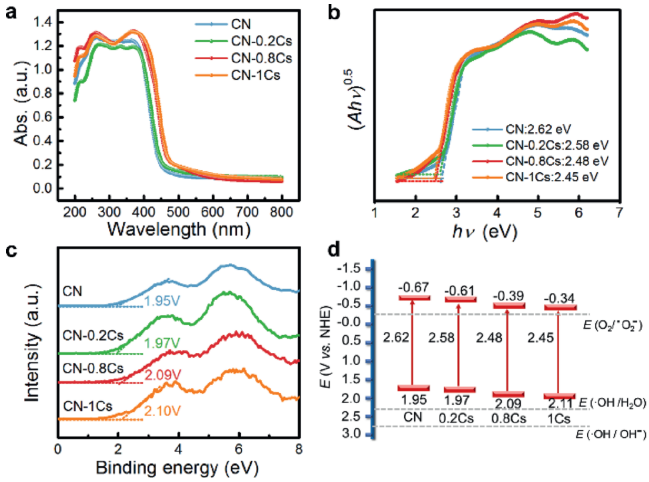

Fig. 3. (a) UV–vis DRS, (b) the estimated band gap, (c) VB XPS, and (d) schematic illustration of the band gap structure of CN and CN-*x*Cs.

conduction band edge and the narrowing of the band gap might be caused by the entry of impurity atoms (Cs and O) and the conjugate effect of C and N atoms, which changed the arrangement of π electrons in the system [30], The introduced N vacancy defect energy would serve as the active site for surface reactions and introduce additional energy levels between the valence band and conduction band of CN [36]. Since the conduction band potentials of CN, CN-0.2Cs, CN-0.8Cs and CN-1Cs were more negative than $E(O_2/{}^{\bullet}O_2^-) = -0.33$ V *vs.* NHE [37], O_2 could be converted into ${}^{\bullet}O_2^-$ during O_2 activation. However, the valence band potentials of CN, CN-0.2Cs, CN-0.8Cs and CN-1Cs were not positive enough to react with H_2O or OH^- to produce ·OH ($E({}^{\bullet}OH/OH^-) = 2.72$ V *vs.* NHE, $E({}^{\bullet}OH/H_2O) = 2.38$ V *vs.* NHE) [37,38].

The effect of Cs doping on the photogenerated electron-hole of the sample on the separation process was studied. As shown in Fig. S4 (Supporting information), CN exhibited a strong and broad PL signal, and after Cs doping, the fluorescence intensity decreased rapidly, indicating that the charge recombination process was inhibited. With the increase of doping concentration, the fluorescence intensity decreased firstly and then increased. The fluorescence intensity of CN-0.8Cs was the lowest and the charge recombination rate was the lowest. The photoelectrochemical

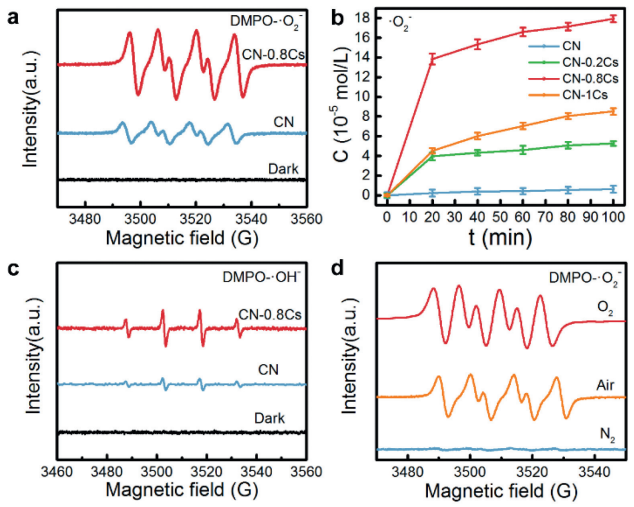

Fig. 4. (a) ESR of DMPO-$^{\bullet}O_2^-$, (b) the amount of $^{\bullet}O_2^-$ tested by color reaction, (c) ESR of DMPO-$^{\bullet}$OH and (d) ESR of DMPO-$^{\bullet}O_2^-$ in different atmospheres.

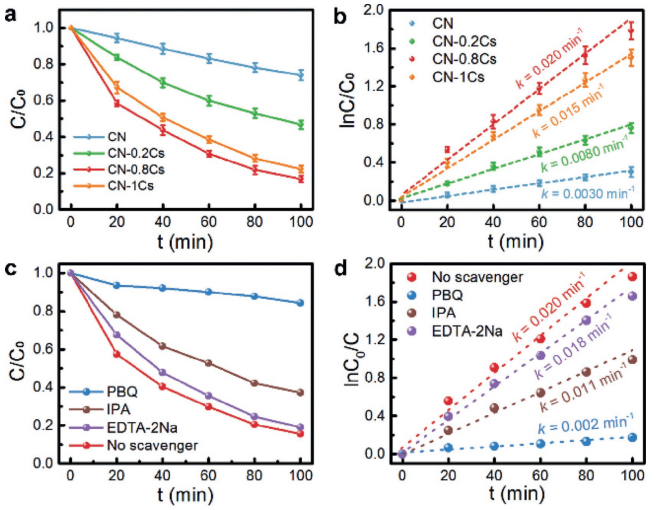

Fig. 5. (a) The photocatalytic degradation curve of CN and CN-*x*Cs for TC solution, (b) *pseudo*-first-order kinetics curve of TC degradation with CN and CN-*x*Cs, (c) photocatalytic efficiency of CN-0.8Cs under different scavenger, and (d) photocatalytic removal of TC by CN-0.8Cs under different scavenger.

measurement was then carried out to further probe the charge separation and transfer ability of the sample. From the transient photocurrent curve given in Fig. S5a (Supporting information), it could be seen that the photocurrent of CN was 0.71 μA. With the increase of Cs doping concentration, the transient photocurrent increased remarkably, showing a trend of first increasing and then decreasing. It reached the maximum at CN-0.8Cs, and the photocurrent was 4.8 μA, which was 6.8 times that of CN. This indicated that the separation and transfer of charge carriers were better after Cs doping. The charge carrier transfer performance of the sample was measured by the EIS in Fig. S5b (Supporting information), and the impedance value was significantly reduced after Cs doping. Among them, CN-0.8Cs showed a smaller curvature, indicating that its charge transfer resistance was lower and it showed better charge transfer performance. The above results indicated that Cs-doped CN exhibited excellent performance in charge carrier separation and transfer. The possible reason was that the doped Cs and the introduction of O could cause distortion of the lattice structure of CN-*x*Cs, resulting in an increase in surface energy, and then the recombination rate of electron-hole pairs decreased [20]. What's more, the doping of Cs might coordinate with N or O atoms to enhance the interaction between adjacent layers, which was beneficial to the transfer of charges between the layers [30]. However, when the doping concentration of Cs was too high, it would seriously damage the CN structure. It was not conducive to the migration of electrons, and the excessive N defects introduced would become the recombination center of electron-hole pairs [36].

The ROS generation ability and source of CN and CN-0.8Cs were tested by the ESR spin trap method (Fig. 4). First, the $^{\bullet}O_2^-$ and $^{\bullet}$OH in the solution were captured by using the capture agent DMPO (5,5-dimethyl-1-pyrroline N-oxide), and then detected by ESR. The shorter-life $^{\bullet}O_2^-$ and $^{\bullet}$OH could form long-life DMPO-$^{\bullet}O_2^-$and DMPO-$^{\bullet}$OH with DMPO. Obviously, the DMPO-$^{\bullet}O_2^-$ adduct had the characteristic that the relative intensity of the four peaks in the ESR spectrum was 1:1:1:1 (Fig. 4a). In the dark, the signal was basically non-existent and signal peaks were observed after illumination. In addition, CN-0.8Cs had a higher signal intensity than CN, indicating that it had a better ability to activate O_2. The quantitative determination of $^{\bullet}O_2^-$ (Fig. 4b) by the color reaction between the sample and NBT under light had further confirmed this point. As can be seen in Fig. 4b, Cs doping can increase the molecular oxygen activation ability. As the doping concentration increases, the molecular oxygen activation ability first increases and then decreases. CN-0.8Cs showed a significantly higher $^{\bullet}O_2^-$ concentration of 179.3 μmol/L, which was much higher than 6.22 μmol/L of CN. Because the doping concentration of CN-1Cs was too high, it had a greater impact on the structure of CN, which was not conducive to the separation and transfer of electrons, inhibiting its molecular oxygen activation ability, leading to its $^{\bullet}O_2^-$ concentration was only 84.6 μmol/L. Furthermore, the detected characteristic signal with a relative intensity of 1:2:2:1 represented the adduct DMPO-$^{\bullet}$OH (Fig. 4c). However, according to Fig. 3d, photogenerated h^+ could not directly react with H_2O or OH^- to generate $^{\bullet}$OH, which meant that $^{\bullet}$OH may be produced by $^{\bullet}O_2^-$, and the path of generation was as follows: $O_2 \rightarrow {}^{\bullet}O_2^- \rightarrow H_2O_2 \rightarrow {}^{\bullet}$OH. The signal intensity of DMPO-$^{\bullet}$OH was much lower than that of DMPO-$^{\bullet}O_2^-$, indicating that $^{\bullet}O_2^-$ was the main reactive species. Subsequently, the signal intensity of DMPO-$^{\bullet}O_2^-$ nitrogen, air, was tested in and oxygen atmospheres (Fig. 4d). In the oxygen atmosphere, the signal strength was found to be the highest, while in the nitrogen environment, the signal strength was negligible, thus confirming the $^{\bullet}O_2^-$ comes from O_2 in the air. Benefiting from the excellent O_2 activation ability, Cs-doped CN was considered to be an efficient photocatalyst for the degradation of organic pollutants. The photocatalytic efficiency of CN and CN-*x*Cs was evaluated by the degradation of TC in an aqueous solution (pH 6.8) under sunlight at room temperature. As shown in Fig. 5a, CN-0.8Cs showed better photocatalytic activity, removing 83.17% TC solution within 100 min, which was remarkably higher than CN (25.96%). Fig. 5b showed the *pseudo*-first order kinetic curve of the degradation of TC solution for all samples. The rate constant k was obtained by calculating the slope of the curve. And the average k value of CN-0.8Cs was 0.020 min^{-1}, which was 6.7 times the degradation rate of CN (k = 0.0030 min^{-1}). This showed that CN-0.8Cs had the most excellent photocatalytic activity. In order to study its stability, the recycling experiment of CN-0.8Cs was carried out (Fig. S6 in Supporting information). After three cycles, the photocatalytic degradation efficiency remained at 70%, which showed that it had reliable stability. Then we test the SEM, TEM, XRD and XPS of the sample after three cycles. As can be seen from Figs. S7-S10 (Supporting information), the chemical structure of the sample had not changed. However, the thickness of the nanosheets increased, the agglomeration was serious, and the Cs content was significantly reduced, resulting in a decrease in the catalytic performance of CN-0.8Cs.

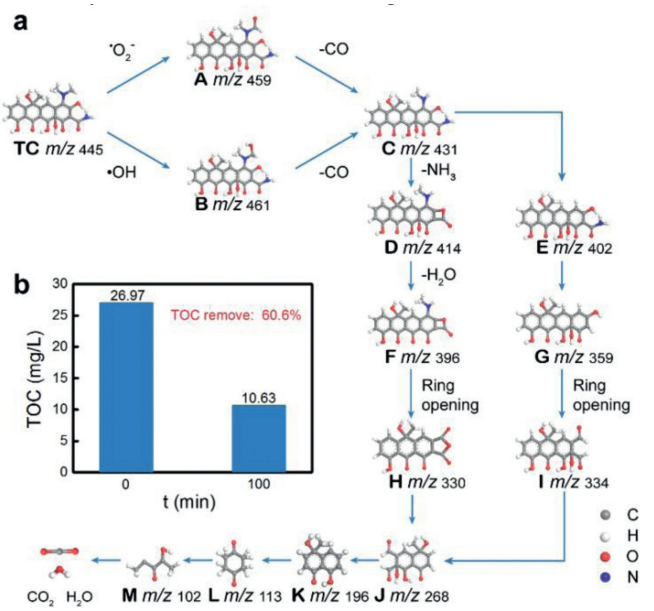

Fig. 6. (a) Proposed degradation pathways of TC by ROS in CN-0.8Cs suspension, and (b) TOC removal of CN-0.8Cs.

The trapping agents were added to the CN-0.8Cs photocatalytic degradation TC solution for capture experiment, so as to calculate the contribution of the active species (h^+, $^{\bullet}O_2^-$ and $^{\bullet}OH$) during the photocatalytic reaction. EDTA-2Na, PBQ and IPA were used as trapping agents for h^+, $^{\bullet}O_2^-$ and $^{\bullet}OH$, respectively [39]. It could be seen from Fig. 5c that the photocatalytic activity was significantly inhibited after adding PBQ, and $^{\bullet}O_2^-$ was the most important active species. In addition, after adding EDTA-2Na, PBQ and IPA, the reaction rate constants (Fig. 5d) were 0.018, 0.0020, and 0.011 min^{-1}, respectively. According to Eq. S3 (Supporting information) [40], the contributions of $^{\bullet}O_2^-$, $^{\bullet}OH$ and h^+ were 90%, 45%, and 10%, respectively.

The thirteen intermediate products (A-M) in the process of CN-0.8Cs photocatalytic degradation of TC were identified by HPLC-MS technology, and the products were shown in Table S6 (Supporting information). Fig. 6a showed a possible way of photocatalytic degradation of TC. Due to the low binding energy of N–C bonds [41–43], it was easy to be attacked by $^{\bullet}O_2^-$ and $^{\bullet}OH$ in photocatalytic oxidation [4], forming intermediates **A** (*m/z* 459) and **B** (*m/z* 461). The CO was subsequently removed to form the product **C** (*m/z* 431). On the one hand, the further loss of $N-CH_3$ in product **C** led to the production of **E** (*m/z* 402). On the other hand, the loss of $-NH_3$ groups in product **C** led to the production of **D** (*m/z* 414). Obviously, **G** (*m/z* 359) was the deamination product of **E**, and **F** (*m/z* 396) was the dehydration product of **D**. As the photocatalytic reaction continues, the benzene ring was gradually opened to form some small molecular products. Finally, the TC in the CN-0.8Cs system was degraded into CO_2 and H_2O, and the corresponding TOC removal efficiency was 60.6%, as shown in Fig. 6b.

In summary, we prepared a high-efficiency photocatalyst of Cs-doped CN by simple heat treatment of CN with CsCl, which was used to study molecular oxygen activation to achieve environmental remediation. The research results suggested that the interaction between CsCl and CN caused the morphology of Cs-doped CN to change, the content of O in the structure increases, and N vacancy defects and cyano groups were formed. The change of physical and chemical structure successfully broadened its light absorption range and promoted the separation and transfer of electrons. Based on these performance improvements, CN-0.8Cs could notably generate high concentration of superoxide radicals $^{\bullet}O_2^-$ (179.30 μmol/L), which was 28.8 times that of CN. However, when the Cs doping concentration was too high, it had a negative effect on the physical and chemical structure of CN, which was not conducive to the separation and transfer of electrons, and inhibited its molecular oxygen activation ability. The results showed that there might be an optimal Cs doping concentration in CN-*x*Cs to achieve high-efficiency O_2 activation.

Declaration of competing interest

The authors declare that they have no known competing financial interests or personal relationships that could have appeared to influence the work reported in this paper.

Acknowledgments

This work is supported by the National Natural Science Foundation of China (Nos. 21872102, 21906001 and 22172080).

Supplementary materials

Supplementary material associated with this article can be found, in the online version, at doi:10.1016/j.cclet.2021.12.089.

References

[1] M. Zhang, C. Lai, B. Li, et al., Chem. Eng. J. 396 (2020) 125343.
[2] Q. Li, F. Li, Chem. Eng. J. 421 (2021) 129915.
[3] H. Li, S. Sun, H. Ji, et al., Appl. Catal. B 272 (2020) 118966.
[4] Z. Zhou, Z. Shen, C. Song, et al., Water Res. 201 (2021) 117314.
[5] J. Xiao, Q. Han, Y. Xie, et al., Environ. Sci. Technol. 51 (2017) 13380–13387.
[6] Y. Cao, Q. Zheng, Z. Rao, et al., Chin. Chem. Lett. 31 (2020) 2689–2692.
[7] N. Tian, H. Huang, X. Du, F. Dong, Y. Zhang, J. Mater. Chem. A 7 (2019) 11584–11612.
[8] C. Wang, M. Fu, J. Cao, et al., Chem. Eng. J. 385 (2020) 123833.
[9] H. Wang, J. Zhang, P. Wang, et al., Chin. Chem. Lett. 31 (2020) 2789–2794.
[10] B. Zhang, C. Li, Y. Zhang, et al., Sci. Total Environ. 757 (2021) 143810.
[11] D. Zhang, X. Han, T. Dong, et al., J. Catal. 366 (2018) 237–244.
[12] X. Hu, P. Lu, Y. He, et al., Appl. Surf. Sci. 528 (2020) 146924.
[13] X. Hu, P. Lu, R. Pan, et al., Chem. Eng. J. 423 (2021) 130278.
[14] X. Liu, W. Yu, C. Li, et al., J. Agric. Food Chem. 69 (2021) 28–35.
[15] X. Li, S. Lyu, X. Lang, Environ. Res. 195 (2021) 110851.
[16] M. Zhang, C. Lai, B. Li, et al., Chem. Eng. J. 422 (2021) 130120.
[17] J. Dai, J. Song, Y. Qiu, et al., ACS Appl. Mater. Interfaces 11 (2019) 10589–10596.
[18] X. Liu, C. Li, Y. Zhang, et al., Appl. Catal. B 219 (2017) 194–199.
[19] L. Lin, H. Ou, Y. Zhang, et al., ACS Catal. 6 (2016) 3921–3931.
[20] W. Yan, L. Yan, C. Jing, Appl. Catal. B 244 (2019) 475–485.
[21] L. Lin, Z. Yu, X. Wang, Angew. Chem. Int. Ed. 131 (2019) 6225–6236.
[22] S. Wu, H. Yu, S. Chen, et al., ACS Catal. 10 (2020) 14380–14389.
[23] Y. Xu, Y. Gong, H. Ren, et al., RSC Adv. 7 (2017) 32592–32600.
[24] K. Mori, D. Tatsumi, T. Iwamoto, et al., Chem. Eur. J. 13 (2018) 1348–1356.
[25] K. Bai, Z. Cui, E. Li, et al., Mod. Phys. Lett. B 34 (2020) 2050361.
[26] H. Zhang, Y. Tang, Z. Liu, et al., Chem. Phys. Lett. 751 (2020) 137467.
[27] B.V. Lotsch, M. Döblinger, J. Sehnert, et al., Chem. Eur. J. 13 (2007) 4969–4980.
[28] S. Cao, J. Low, J. Yu, et al., Adv. Mater. 27 (2015) 2150–2176.
[29] P. Niu, L. Zhang, G. Liu, H. Cheng, Adv. Funct. Mater. 22 (2012) 4763–4770.
[30] T. Xiong, W. Cen, Y. Zhang, F. Dong, ACS Catal. 6 (2016) 2462–2472.
[31] G. Zhang, G. Li, Z. Lan, et al., Angew. Chem. Int. Ed. 56 (2017) 13445–13449.
[32] H. Lan, L. Li, X. An, et al., Appl. Catal. B 204 (2017) 49–57.
[33] C. Chang, Y. Fu, M. Hu, et al., Appl. Catal. B 142 (2013) 553–560.
[34] X.L. Wang, W.Q. Fang, N. Abbas, et al., J. Mater. Chem. A 1 (2013) 14089–14096.
[35] V.W. Lau, V.W. Yu, F. Ehrat, et al., Adv. Energy Mater. 7 (2017) 1602251.
[36] H. Yu, R. Shi, Y. Zhao, et al., Adv. Mater. 29 (2017) 1605148.
[37] L. Luo, T. Zhang, M. Wang, et al., ChemSusChem 13 (2020) 5173–5184.
[38] W. Zhang, L. Zhou, J. Shi, et al., J. Colloid Interface Sci. 496 (2017) 167–176.
[39] P. Qiu, C. Xu, H. Chen, et al., Appl. Catal. B 206 (2017) 319–327.
[40] P. Chen, L. Blaney, G. Cagnetta, et al., Environ. Sci. Technol. 53 (2019) 1564–1575.
[41] S. Jiao, S. Zheng, D. Yin, L. Wang, L. Chen, Chemosphere 73 (2008) 377–382.
[42] B. Balci, N. Oturan, R. Cherrier, et al., Water Res. 43 (2009) 1924–1934.
[43] V.M. Mboula, V. Hequet, Y. Gru, et al., J. Hazard. Mater. 209 (2012) 355–364.